Am J Cancer Res 2026;16(5):1696-1712
www.ajcr.us /ISSN:2156-6976/ajcr0171903

Original Article

Integrated gene expression profiling identifies key molecular drivers and a predictive signature for malignant transformation of oral lichen planus to squamous cell carcinoma

Bingjie Wang[1], Mengzhe Cai[1], Luyi Chai[1], Qiang Xie[2]

[1]*Department of Stomatology, The Affiliated People's Hospital of Ningbo University, Ningbo 315000, Zhejiang, China;* [2]*Department of Medical Record, The Affiliated People's Hospital of Ningbo University, Ningbo 315000, Zhejiang, China*

Received February 5, 2026; Accepted March 25, 2026; Epub May 15, 2026; Published May 30, 2026

Abstract: Chronic oral inflammation plays a crucial role in the malignant transformation of oral lichen planus (OLP) to oral squamous cell carcinoma (OSCC). This study aims to identify the key molecular characteristics related to chronic inflammation, OLP and OSCC. Integrate the gene expression data set of chronic oral inflammation, OLP and OSCC to identify common differential expression genes (DEGs). Carry out functional enrichment, protein-protein interaction (PPI) analysis, LASSO-logistic regression model, quantitative detection of inflammatory mediators and correlation analysis. It was verified in cell models and clinical tissue samples through real-time quantitative polymerase chain reaction (qRT-PCR). Through comprehensive analysis, we have identified 13 differential expression genes (DEG), which are persistently dysfunctional in chronic inflammation, OLP and OSCC pathological states, among which PTGS2, PLAUR, ERRFI1 and ODC1 are particularly critical. Based on this, we have constructed a malignant transformation prediction model of PLAUR, ERRFI1 AND ODC1. The model showed excellent effectiveness in distinguishing disease states, with an area under the curve (AUC) reaching 0.93. qRT-PCR results show that compared with normal oral epithelial cells, PLAUR, ERRFI1 and ODC1 are significantly upre-regulated ($P < 0.01$ or $P < 0.001$) in immune-stimulated simulated inflammatory environments and OSCC cells, among which they are observed in immune-stimulated cells. To the highest level of expression. The inflammatory mediators TNF-α, IL-1 and IL-6 also showed a consistent upward trend in the above cell models ($P < 0.05$). Correlation analysis shows that the expression of these three key genes is significantly positively correlated with the concentration of TNF-α, IL-1 and IL-6. Clinical tissue sample verification showed that the expression of ODC1, PLAUR and ERRFI1 in the normal mucosa was significantly lower than that of OLP foci and OSCC tissue, and the expression in OLP was significantly lower than that of OSCC tissue ($P < 0.05$). Gene expression characteristics composed of genes such as PLAUR, ERRFI1 and ODC1 can shows promising predictive capability the risk of OLP malignancy and provide new potential targets for intervention treatment.

Keywords: Oral lichen planus, oral squamous cell carcinoma, chronic inflammation, malignant transformation, biomarkers, bioinformatics

Introduction

Oral lichen planus (OLP) is a chronic inflammatory mucosal disease with a global prevalence of about 1-2%. Clinically, its main characteristics are white stripes, erythema or ulcers. It is considered a potentially malignant disease, and about 1-2% of cases progress to oral squamous cell carcinoma (OSCC) [1, 2]. OSCC is one of the primary malignant tumors of the head and neck, with more than 350,000 new diagnosed cases worldwide every year, and the five-year survival rate is less than 50% [3]. Chronic oral inflammation is a key precursor to the development of OLP and OSCC, which may induce tumor microenvironment through abnormal gene expression involving key signaling pathways [4, 5]. Understanding the molecular continuum from chronic inflammation to OLP and ultimately to OSCC is critical for identifying

https://doi.org/10.62347/PPHC9996

early warning biomarkers and intervention targets. However, systematic investigation of gene expression changes across these three sequential pathological states remains limited. OLP is classified as an oral potentially malignant disorder (OPMD) with a reported malignant transformation rate of approximately 1-2% [6]. However, current clinical practice lacks reliable molecular biomarkers to identify which OLP patients are at highest risk of progressing to OSCC. This gap in early warning capability often leads to either unnecessary aggressive intervention or delayed diagnosis of malignant transformation, highlighting an urgent unmet clinical need. In this study, we integrated transcriptomic data from chronic oral inflammation, OLP lesions, and OSCC tissues to identify persistently dysregulated genes that may drive the inflammation-to-cancer progression.

Recent research has focused on early biomarkers and gene expression changes associated with the conversion of OLP into OSCC [7, 8]. According to a study by Sarinthon et al., significant differences in the expression of cell adhesion molecule CD146 were observed between OLP and OSCC tissues. Specifically, CD146 expression is elevated in OLP lesions and reduced in cancerous tissue, indicating that it may participate in the immunomodulation mechanism in the process of early malignant transformation [9]. The bioinformatics analysis of another study showed that the FAM3B gene was down-regulation in OLP tissue, and its expression was further reduced when it progressed to malignant tumors. Furthermore, FAM3B expression deficiency is significantly associated with tumor progression and poor prognosis in patients, making it a potential biomarker for predicting malignant transformation in OLP patients [10]. In addition, Cristóvão and others. Using high-throughput RNA sequencing combined with epigenetic analysis, it was revealed that the expression level of interleukin 1β and hypoxic inducing factor 1α, the chronic inflammatory-related genes in OLP lesions, was significantly increased, and further increased in OSCC tissue. Carmen and others. It is proposed that the chronic inflammation of OLP may promote a tumor-like microenvironment conducive to gene mutation and abnormal accumulation, and ultimately drive malignant transformation [11]. In fact, chronic inflammation is considered a sign of promoting tumor inflammation [12]. Its characteristic feature is the persistent stimulation of mucosal epithelium and immune cells, triggering the secretion of multiple cytokines and growth factors. These media induce excessive proliferation of cells, inhibit apoptosis, and lead to genomic instability, creating favorable conditions for malignant transformation. Although these studies provide supporting evidence of the association between OLP and OSCC, the exact molecular mechanism of this progression mediated by chronic inflammation remains unclear. This ambiguity hinders the development of early diagnosis strategies and targeted treatment interventions. Based on this, this study aims to systematically clarify the molecular mechanism of chronic inflammation-driven OLP malignancy and identify key genes through the combination of bioinformatics analysis and experimental verification. This method aims to provide molecular targets and theoretical basis for early risk warning and precise intervention of OLP patients.

Methods

Data collection and preprocessing

This study uses gene expression spectrum data from three public datasets in NCBI's GEO database: GSE28035 (chronic oral inflammation model, containing 6 samples from dental pulpitis patients and 6 healthy controls, total n = 12; platform: Affymetrix Human Genome U133 Plus 2.0 Array), GSE52130 (OLP, comprising 9 OLP lesion samples and 6 normal oral mucosal samples, total n = 15; platform: Illumina HumanHT-12 V4.0 expression BeadChip array), and GSE74530 (OSCC, including 6 OSCC tumor tissues and 6 matched normal controls, total n = 12; platform: Affymetrix Human Genome U133 Plus 2.0 Array). This sequential selection enables investigation of the molecular continuum from initial inflammation, through premalignant OLP, to established malignancy. Use the GEOquery package in R software to download the original data. Quality control and standardization of data sets from different experimental batches and platforms. For microarray data sets, use the robust multi-array average (RMA) method or the standard procedure provided by the original research for background correction and standardization.

The probe ID is mapped to the genetic symbol, and the probe with low expression level or sig-

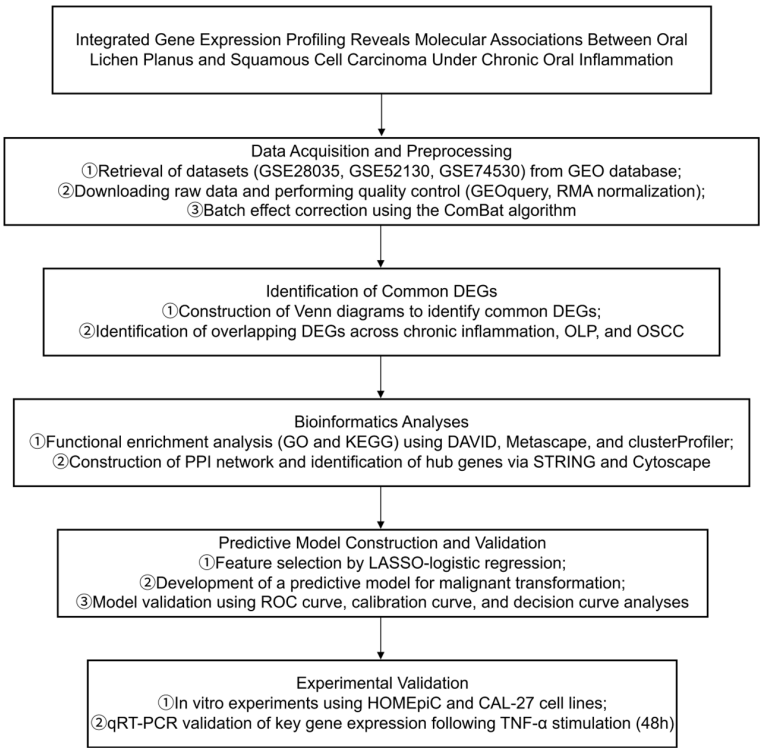

Figure 1. Comprehensive bioinformatics analysis and experimental verification flowchart to determine the key molecular link between OLP and OSCC in chronic oral inflammation.

nificant noise is removed. In order to explain the differences between multiple experimental batches and platforms, use ComBat or similar algorithms to correct the batch effect. To preserve biological variation, sample type (normal, inflammatory, OLP, OSCC) was included in the ComBat model as a covariate. After preprocessing and batch effect correction, a comparable gene expression matrix is generated for each data set, which lays the foundation for subsequent differential expression analysis. **Figure 1** shows the detailed workflow.

Differential expression analysis

DEGs identified in chronic oral inflammation, OLP, and OSCC groups. For dataset GSE28035, gene expression was compared between chronic inflammatory stimulation conditions and control conditions. In dataset GSE52130, DEGs were analyzed between OLP lesions and normal oral mucosal epithelium; in GSE74530, DEGs were identified by comparing OSCC tumor tissues with matched normal controls. Analysis of differential expression employed R/Bioconductor limma or online GEO2R, control FDR via multiple testing; adj. $P < 0.05$ & $|\log2FC| \geq 1$ genes are DEGs. Volcano plots and clustering heatmaps visualized the results of differential expression analysis to intuitively display overall gene expression patterns within each group and highlight variation between samples.

Identification of common differentially expressed genes

Intersect the DEG sets identified in the above three comparisons to identify common DEGs that persist under chronic inflammation, OLP and OSCC conditions. Draw a Vien diagram to visualize the overlap between these DEG sets. Pay special attention to the list of genes from triple cross, because these genes may represent the key molecular mediators that drive the malignant conversion of OLP under chronic inflammation. Further check the expression patterns of these common DEGs under each condition (the consistency of up or down). In addition, the functional correlation between these genes and inflammatory response or tumor development is evaluated according to the current literature.

Functional enrichment and pathway analysis

Analyze identified common DEGs via GO and KEGG pathway enrichment. Use bioinformatics tools such as DAVID, Metascape and R-pack clusterProfiler for enrichment analysis, focusing on biological processes, cell composition, molecular functions and significantly enriched signaling pathways. These analyses aim to clarify the functional role of common DEG in chronic inflammation and tumor development.

Construction of protein-protein interaction (PPI) network

Investigate protein-protein interactions (PPIs) among co-expressed differentially expressed genes (DEGs) using the online STRING database. Construct an initial PPI network by select-

ing an appropriate confidence threshold and visualize interactions using Cytoscape software. Apply network analysis algorithms to identify key hub genes within the network. Hub genes typically represent highly interconnected nodes mediating numerous interactions, indicating their central importance in biological processes. Through these steps, several key hub genes were identified that may play a critical role in chronic inflammation-driven carcinogenesis.

Identification of key genes and prognostic analysis

For LASSO-logistic regression analysis, we utilized the OSCC dataset GSE74530 as the discovery cohort, which contains 6 OSCC tumor samples and 6 matched normal controls (total n = 12). This is despite the fact that this sample size is relatively small and below the commonly recommended rule of thumb of at least 10 sample sizes per predictor. However, LASSO regression is suitable for high-dimensional data with limited sample sizes because its L1 regularization penalty inherently reduces the risk of overfitting by shrinking the coefficients and performing automatic feature selection. To assess the stability of the model, LASSO regression was performed using the glmnet package in R with 10-fold cross-validation to determine the optimal penalty parameter λ. The λ value minimizing the cross-validation error (λ.min) was selected for feature selection, retaining genes with non-zero coefficients as predictive biomarkers. Subsequently, a multivariate logistic regression model was constructed using these selected genes to estimate the probability of malignant transformation. Model performance was evaluated by area under the receiver operating characteristic curve (AUC), calibration curve (assessing agreement between predicted and observed probabilities), and decision curve analysis (evaluating clinical net benefit across threshold probabilities). In decision curve analysis, a range of 0.05 to 0.75 was selected to cover clinically meaningful risk levels for malignant transformation in OLP patients: thresholds below 0.05 are typically considered too low to trigger clinical action, while thresholds above 0.75 represent very high risk where intervention is almost always warranted.

Establishment of OLP-like inflammatory cell model in vitro

To simulate the immune-inflammatory microenvironment characteristic of oral OLP, a T cell-keratinocyte co-culture model was established. Briefly, normal human oral epithelial cells (HOMEpic) were cultured in keratinocyte growth medium at 37°C with 5% CO_2, followed by pretreatment with IFN-γ (10 ng/mL, PeproTech, USA) for 24 h to enhance antigen-presenting capacity. Human T cells were isolated from healthy donor peripheral blood mononuclear cells (PBMCs) using Ficoll density gradient centrifugation and negative magnetic selection from Miltenyi Biotec (Germany). T cells were activated with lectin for 24 hours. Activated T cells were co-cultured with IFN-γ-pretreated HOMEpic cells at a 5:1 ratio (T cells: keratinocytes) and simultaneously stimulated with TNF-α (10 ng/mL) and IL-17 (50 ng/mL, PeproTech, USA) for an additional 48 h. Untreated HOMEpic cells served as controls. The cells were subsequently collected, followed by extraction of total RNA for qRT-PCR analysis.

Normal human oral epithelial cells (HOMEpic) were purchased from ScienCell Research Laboratories (Catalog #2620, Carlsbad, CA, USA). Cells were cultured in Oral Epithelial Cell Medium (OEpiCM, Catalog #2611, ScienCell) supplemented with 1% Oral Epithelial Cell Growth Supplement, 1% penicillin/streptomycin solution, and 10% fetal bovine serum at 37°C in a humidified atmosphere with 5% CO_2. Cells from passages 3-5 were used for all experiments.

Validation of key genes by experimental assays

Based on the comprehensive analysis of differential expression, functional enrichment, and logistic regression model, three key genes (ODC1, PLAUR, and ERRFI1) were selected for experimental validation [11]. Total RNA was extracted from three groups of cells (normal HOMEpic, immune-stimulated HOMEpic, and CAL-27 cells) using TRIzol reagent (Invitrogen, USA). RNA concentration and purity were measured using a NanoDrop spectrophotometer. cDNA was synthesized from 1 μg total RNA using HiScript II Q RT SuperMix (Vazyme Biotech, China, Cat# R223-01). qRT-PCR was

performed using AceQ Universal SYBR qPCR Master Mix (Vazyme Biotech, Cat# Q711-02, batch# 7E3710) on a StepOnePlus Real-Time PCR System (Applied Biosystems, USA). The primer sequences were as follows: ODC1: F: 5'-TTGGCAGCTAGATGTGTCCT-3', R: 5'-CACAAGAGCTGCATGGAACT-3'; PLAUR: F: 5'-TGTAAGACCAACGGGGATTG-3', R: 5'-AGCCAGTCCGATAGCTCAGG-3'; ERRFI1: F: 5'-GCTGGAGTCTGTGCTGAATG-3', R: 5'-CTTCACACTGGCGATGGTAG-3'; GAPDH: F: 5'-GGAGCGAGATCCCTCCAAAAT-3', R: 5'-GGCTGTTGTCATACTTCTCATGG-3'.

All primers were synthesized by Sangon Biotech (Shanghai, China). The reaction system (20 μL) consisted of: 10 μL SYBR qPCR Master Mix, 0.4 μL each of forward and reverse primers (10 μM), 2 μL cDNA, and 7.2 μL RNase-free ddH_2O. Thermal cycling conditions were: 95°C for 5 min, followed by 40 cycles of 95°C for 10 sec and 60°C for 30 sec. A melting curve analysis was performed to verify primer specificity. Each sample was analyzed in triplicate (three technical replicates), and three independent biological replicates were performed for each group. Relative mRNA expression levels were calculated using the 2^-ΔΔCt method with GAPDH as the internal reference.

Quantification of inflammatory cytokines and correlation analysis

Cell culture supernatants were collected from three experimental groups: normal HOMEpic cells, immune-stimulated HOMEpic cells, and CAL-27 OSCC cells. The levels of TNF-α, IL-1β, and IL-6 were measured using commercial enzyme-linked immunosorbent assay (ELISA) kits according to the manufacturer's instructions. The following kits were used: (1) Human TNF-α Quantikine ELISA Kit (R&D Systems, Minneapolis, USA, Cat# DTA00D, batch# P247815); (2) Human IL-1β/IL-1F2 Quantikine ELISA Kit (R&D Systems, Cat# DLB50, batch# P249326); (3) Human IL-6 Quantikine ELISA Kit (R&D Systems, Cat# D6050, batch# P251437).

Each sample was measured in duplicate, and three independent biological replicates were performed for each group. The absorbance was read at 450 nm using a microplate reader (BioTek, USA). Cytokine concentrations were calculated from standard curves. Pearson correlation analysis was performed to assess the relationship between mRNA expression levels of ODC1, PLAUR, and ERRFI1 and the concentrations of TNF-α, IL-1β, and IL-6.

Validation in clinical tissue samples

This study was approved by the Ethics Committee of the Affiliated People's Hospital of Ningbo University (Approval No. Ning Da Fu Ren Lun examination 2025 research No. 078). All patients provided written informed consent prior to participation. Inclusion criteria for OLP patients: (1) Histopathologically confirmed diagnosis of OLP according to WHO criteria; (2) No prior history of malignant tumors; (3) No prior radiotherapy or chemotherapy. Exclusion criteria: (1) Patients with lichenoid reactions to drugs or dental materials; (2) Patients with other oral potentially malignant disorders; (3) Insufficient tissue sample for analysis.

In order to further confirm the translational relevance of our findings, an independent clinical tissue sample cohort was used for validation. Archived FFPE tissue blocks were provided by the pathology department. The cohort consists of three groups: normal oral mucosa (NOM, n = 6), histologically confirmed OLP lesions (n = 6), and primary OSCC tissue (n = 6), with a total of 18 samples. This validation cohort is completely independent from the discovery cohort (GSE74530) used for LASSO modeling. Total RNA was extracted from ten 10 μm FFPE sections using the RNeasy FFPE Kit (Qiagen, Hilden, Germany), which is optimized for recovery of degraded RNA from archival tissues. Subsequently, the relative mRNA expression levels of ODC1, PLAUR, and ERRFI1 were measured by qRT-PCR as described in Section 2.8, with GAPDH as the internal reference. Expression levels were compared among the three clinical groups.

Statistical analysis

All statistical analyses were performed using R software (version 4.2.0) and GraphPad Prism (version 9.0). Data are presented as mean ± standard deviation (SD). For comparisons between two groups, Student's t-test was used. For multiple group comparisons, one-way ANOVA followed by Tukey's post-hoc test was applied. Pearson correlation analysis was used to assess correlations between gene expression and cytokine levels. A P-value < 0.05 was considered statistically significant. For all

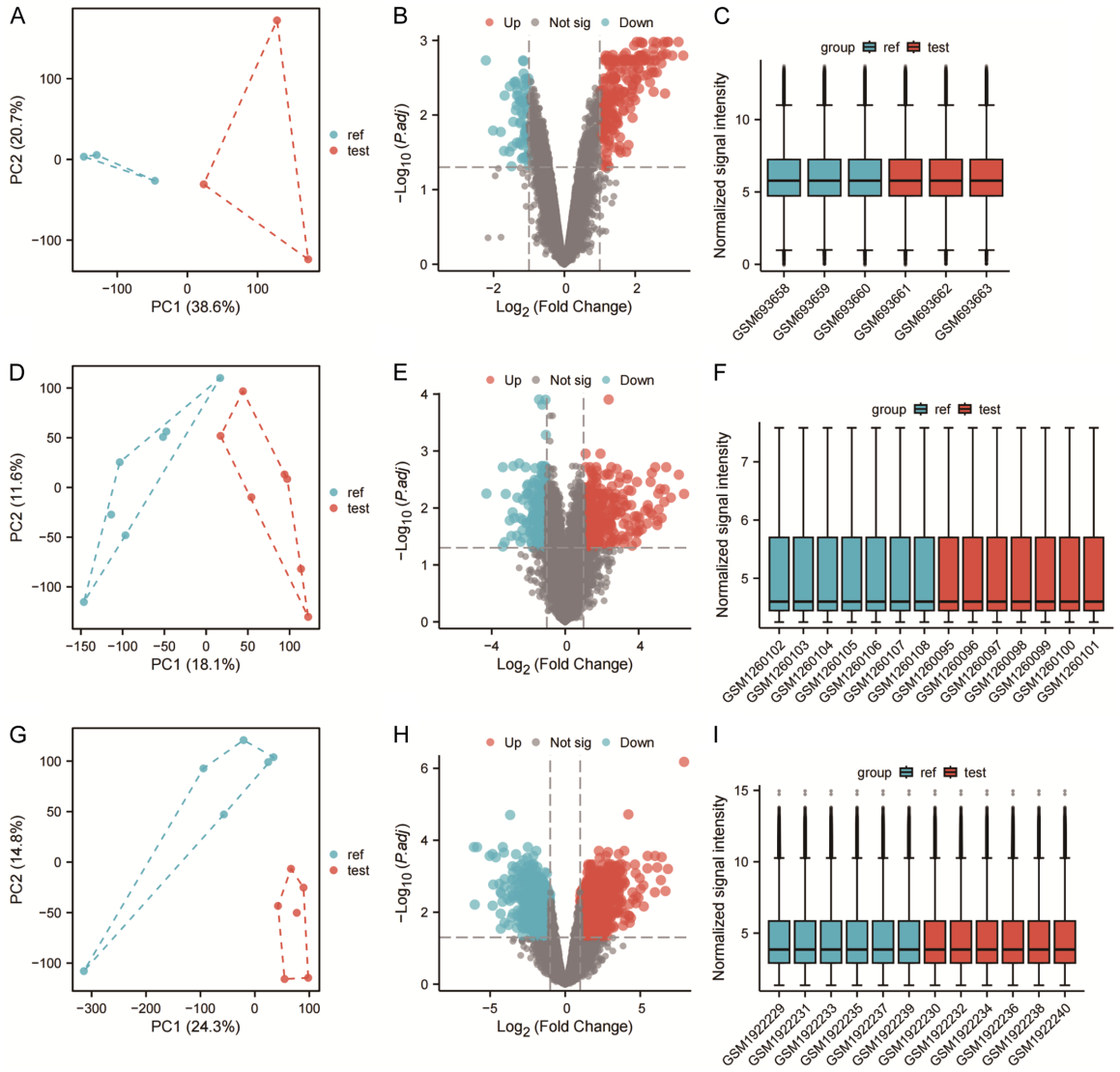

Figure 2. Quality control and differential expression analysis across the disease continuum from chronic inflammation to OLP to OSCC. A. PCA clustering of chronic oral inflammation samples (n = 6) versus controls (n = 6). B. Volcano plot of differentially expressed genes between chronic oral inflammation and controls (|log2FC| ≥ 1, adj.P < 0.05). C. Boxplot of standardized signal intensity after preprocessing the chronic inflammation dataset, showing balanced data distribution. D. PCA clustering of OLP lesions (n = 9) versus normal mucosa controls (n = 6). E. Volcano plot of differentially expressed genes between OLP and normal mucosa (|log2FC| ≥ 1, adj.P < 0.05). F. Boxplot of standardized signal intensity after preprocessing the OLP dataset. G. PCA clustering of OSCC tumor samples (n = 6) versus normal mucosa controls (n = 6). H. Volcano plot of differentially expressed genes between OSCC and normal mucosa (|log2FC| ≥ 1, adj.P < 0.05). I. Boxplot of standardized signal intensity after preprocessing the OSCC dataset.

experiments, at least three independent biological replicates were performed.

Results

Quality control and differential expression analysis of gene expression data

Quality control and differential expression analysis were performed on the chronic oral inflammation, OLP, and OSCC datasets, respectively (**Figure 2**). In the chronic inflammation dataset, PCA results showed clear separation between samples and controls (**Figure 2A**; PC1 = 38.6%, PC2 = 20.7%). The volcano plot indicated slightly more upregulated than downregulated genes among differentially expressed genes (**Figure 2B**), while box plots demonstrated balanced data distribution without significant batch effects (**Figure 2C**). In the OLP dataset, PCA dis-

tinguished lesions from normal samples (**Figure 2D**; PC1 = 18.1%, PC2 = 11.6%), the volcano plot showed comparable numbers of up- and downregulated genes (**Figure 2E**), and the boxplot reflected good normalization (**Figure 2F**). In the OSCC dataset, PCA clearly distinguished cancerous from normal tissues (**Figure 2G**; PC1 = 24.3%, PC2 = 14.8%). The volcano plot showed the highest number of differentially expressed genes with the greatest fold change (**Figure 2H**), while the boxplot confirmed stable data after correction (**Figure 2I**).

Key differential gene signatures and pathway enrichment characteristics

Figure 3 displays the differentially expressed genes and functional enrichment results between each disease group and normal mucosa. **Figure 3A** (chronic inflammation heatmap) reveals upregulation of immune-related genes such as Cxcl10, Ccl8, and Zbtb16 in inflammatory samples, with lower expression in the control group. **Figure 3B** (GSEA) indicates significant negative enrichment of the "Cell Cycle" and "Cell Cycle Mitosis" pathways (minimum enrichment score ~0.6). **Figure 3C** (OLP Heatmap) presents a dual-cluster expression pattern: keratin genes (e.g., KRT1, KRT10) are upregulated, while ECM regulatory genes are downregulated. **Figure 3D** (GSEA) shows significant positive enrichment of the "Keratinization" and "Keratinization-related envelope formation" pathways (peak enrichment score ~0.8). **Figure 3E** (OSCC heatmap) shows significant upregulation of ECM components (e.g., COL1A1, MMPs, FN1) and downregulation of some epithelial differentiation genes. **Figure 3F** (GSEA) indicates significant enrichment of the "extracellular matrix organization" and "collagen formation" pathways (peak > 0.6).

Common intersection genes reveal shared hubs in inflammation-carcinogenesis axis and their predictive potential

Through intersection analysis of differentially expressed genes in chronic inflammation, OLP, and OSCC (**Figure 4**), the Venn diagram (**Figure 4A**) revealed 13 genes co-expressed across all three groups, all of which met the predefined DEG screening criteria (adj. $P < 0.05$ and $|\log2FC| \geq 1$) in each respective comparison. Additionally, 8, 72, and 281 overlapping genes were identified between inflammation and OLP, inflammation and OSCC, and OLP and OSCC, respectively, with each group exhibiting numerous condition-specific expression genes. Protein interaction network analysis (**Figure 4B**) grouped these 13 intersecting genes into two interaction modules: one centered around PTGS2, including genes such as PLAUR and ODC1; the other composed of CCN2, PTHLH, and others. Functional associations were established through connections between PTGS2 and CCN2. Functional enrichment analysis (**Figure 4C**) revealed that these genes were primarily enriched in biological processes such as cyclic nucleotide metabolism and keratinocyte differentiation regulation. In cellular components, they were enriched in structures like membrane rafts/pits, while molecular functions included IGF receptor binding and cAMP phosphodiesterase activity. KEGG pathways showed significant enrichment only in "adipocyte lipolysis regulation".

The PPI network revealed two functionally distinct modules with important clinical implications. Module 1, centered around PTGS2 (COX-2) and including PLAUR and ODC1, represents an "inflammation-proliferation module". COX-2 is a well-established therapeutic target for chemoprevention, while ODC1 is the target of difluoromethylornithine (DFMO), a chemopreventive agent already tested in oral cancer trials. Module 2, comprising CCN2 and PTHLH, constitutes an "ECM-growth factor module" associated with tumor invasion and bone destruction, which are clinically relevant features of advanced OSCC. The KEGG pathway "regulation of lipolysis in adipocytes", although seemingly peripheral, may reflect the metabolic reprogramming associated with cancer progression and could have implications for tumor-stroma interactions.

ROC curve analysis (**Figure 4D**, **4E**) revealed that most genes demonstrated good discriminatory ability. Among them, ERRFI1, PTHLH, CLDN23, ODC1, and IRS1 all had AUC values ≥ 0.94, while genes such as DUSP6, ELF3, and CTGF had AUC values between 0.81 and 0.92, and PDE4B had an AUC value of approximately 0.61. The functional distribution of these genes is summarized in **Table 1**.

Among the 13 common DEGs, 12 genes (PTGS2, ERRFI1, PDE4B, PTHLH, DUSP6, ELF3, CTGF, FBN2, ABCA12, ODC1, IRS1, and PLAUR)

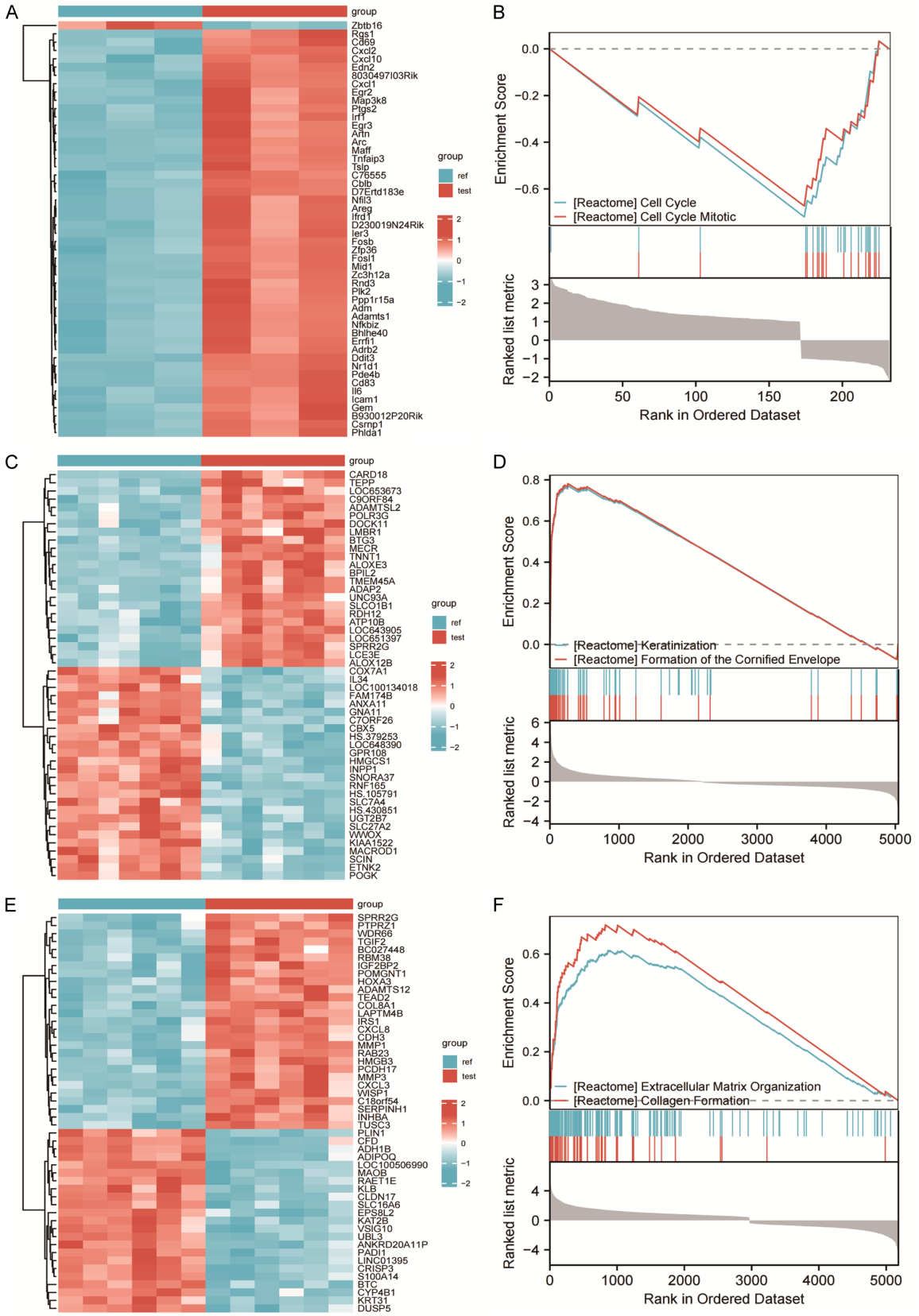
A
group
Zbtb16
Rgs1
Cd69
Cxcl2
Cxcl10
Edn2
8030497I03Rik
Cxcl1
Egr2
Map3k8
Ptgs2
Irf1
Egr3
Arh
Arc
Maff
Tnfaip3
Tslp
C76555
Cblb
D7Ertd183e
Nfil3
Areg
Ifrd1
D230019N24Rik
Ier3
Fosb
Zfp36
Fosl1
Mid1
Zc3h12a
Rnd3
Plk2
Ppp1r15a
Adm
Adamts1
Nfkbiz
Bhlhe40
Errfi1
Adrb2
Ddit3
Nr1d1
Pde4b
Cd83
Il6
Icam1
Gem
B930012P20Rik
Csrnp1
Phlda1
group
ref
test
2
1
0
−1
−2
B
Enrichment Score
0.0
−0.2
−0.4
−0.6
[Reactome] Cell Cycle
[Reactome] Cell Cycle Mitotic
Ranked list metric
3
2
1
0
−1
−2
0
50
100
150
200
Rank in Ordered Dataset
C
group
CARD18
TEPP
LOC653673
C9ORF84
ADAMTSL2
POLR3G
DOCK11
LMBR1
BTG3
MECR
TNNT1
ALOXE3
BPIL2
TMEM45A
ADAP2
UNC93A
SLCO1B1
RDH12
ATP10B
LOC643905
LOC651397
SPRR2G
LCE3E
ALOX12B
COX7A1
IL34
LOC100134018
FAM174B
ANXA11
GNA11
C7ORF26
CBX5
HS.379253
LOC648390
GPR108
HMGCS1
INPP1
SNORA37
RNF165
HS.105791
SLC7A4
HS.430851
UGT2B7
SLC27A2
WWOX
KIAA1522
MACROD1
SCIN
ETNK2
POGK
group
ref
test
2
1
0
−1
−2
D
Enrichment Score
0.8
0.6
0.4
0.2
0.0
[Reactome] Keratinization
[Reactome] Formation of the Cornified Envelope
Ranked list metric
6
4
2
0
−2
−4
0
1000
2000
3000
4000
5000
Rank in Ordered Dataset
E
group
SPRR2G
PTPRZ1
WDR66
TGIF2
BC027448
RBM38
IGF2BP2
POMGNT1
HOXA3
ADAMTS12
TEAD2
COL8A1
LAPTM4B
IRS1
CXCL8
CDH3
MMP1
RAB23
HMGB3
PCDH17
MMP3
CXCL3
WISP1
C18orf54
SERPINH1
INHBA
TUSC3
PLIN1
CFD
ADH1B
ADIPOQ
LOC100506990
MAOB
RAET1E
KLB
CLDN17
SLC16A6
EPS8L2
KAT2B
VSIG10
UBL3
ANKRD20A11P
PADI1
LINC01395
CRISP3
S100A14
BTC
CYP4B1
KRT31
DUSP5
group
ref
test
2
1
0
−1
−2
F
Enrichment Score
0.6
0.4
0.2
0.0
[Reactome] Extracellular Matrix Organization
[Reactome] Collagen Formation
Ranked list metric
4
0
−4
0
1000
2000
3000
4000
5000
Rank in Ordered Dataset

Figure 3. Differential gene expression and pathway enrichment analysis across chronic inflammation, OLP, and OSCC compared to normal controls. A. Heatmap of differentially expressed genes between chronic oral inflammation samples (n = 6) and controls (n = 6), showing upregulation of immune-related genes. B. Gene set enrichment analysis (GSEA) plot showing significant negative enrichment of cell cycle-related pathways in chronic inflammation (normalized enrichment score [NES] < -0.6, false discovery rate [FDR] < 0.05). C. Heatmap of differentially expressed genes between OLP lesions (n = 9) and normal mucosa controls (n = 6), revealing dual-cluster expression pattern of keratin and ECM regulatory genes. D. GSEA plot showing significant positive enrichment of keratinization-related pathways in OLP (NES > 0.8, FDR < 0.05). E. Heatmap of differentially expressed genes between OSCC tumor samples (n = 6) and normal mucosa controls (n = 6), showing upregulation of ECM components. F. GSEA plot showing significant enrichment of extracellular matrix organization and collagen formation pathways in OSCC (NES > 0.6, FDR < 0.05).

exhibited consistent upregulation across chronic inflammation, OLP, and OSCC compared to their respective normal controls. In contrast, CLDN23 showed consistent downregulation in all three conditions. This uniform directional trend - with the majority of genes persistently upregulated and only CLDN23 downregulated - supports their potential role as stable molecular drivers along the inflammation-OLP-OSCC continuum.

Risk prediction model for malignant transformation

To address the risk of overfitting due to the small sample size (n = 12), we performed 10-fold cross-validation repeated 10 times. The model achieved a mean cross-validated AUC of 0.89 (SD = 0.06), supporting the robustness of the feature selection despite the limited sample size. The cross-validation curve (**Figure 5A**) indicates that partial likelihood bias is minimized when $\log(\lambda) \approx -2.1$, at which point the model retains three genes with non-zero coefficients. The coefficient trajectory plot (**Figure 5B**) further confirms PLAUR, ERRFI1, and ODC1 as the final selected features. Based on these three genes, a scattering diagram was constructed (**Figure 5C**). ROC analysis (**Figure 5D**) shows that the model AUC is 0.93 (95% CI: 0.85-1.00). The calibration curve (**Figure 5E**) shows that the prediction probability is closely related to the results observed diagonally, and the average absolute error is about 0.07. Decision curve analysis (**Figure 5F**) indicates that within the threshold probability range of 0.05-0.75, the model significantly outperforms both “treat all” and “treat none” strategies.

Experimental validation of key genes in cell models and clinical samples

qRT-PCR was performed to measure mRNA expression levels of ODC1, PLAUR, and ERRFI1 in both in vitro cell models and independent clinical tissue samples. As shown in **Figure 6A**, compared with normal HOMEpic cells, all three genes were significantly upregulated in immune-stimulated oral epithelial cells ($P < 0.01$ for ODC1 and PLAUR; $P < 0.001$ for ERRFI1) and in CAL-27 OSCC cells ($P < 0.01$ or $P < 0.001$). Notably, immune-stimulated cells exhibited even higher expression than CAL-27 cells for ERRFI1 ($P < 0.001$) and for ODC1 and PLAUR ($P < 0.05$). In clinical tissue samples (**Figure 6B**), a gradient increase in expression was observed across the disease continuum: normal mucosa showed the lowest expression, OLP lesions showed intermediate levels, and OSCC tissues exhibited the highest expression of all three genes ($P < 0.05$ for all comparisons).

Experimental analysis of inflammatory factors TNF-α, IL-1, and IL-6 levels in vitro

As shown in **Figure 7**, the expression levels of TNF-α, IL-1, and IL-6 were detected in normal oral epithelial cells (HOMEpic), oral squamous carcinoma cells (CAL-27), and immunostimulated HOMEpic cells. Compared with normal HOMEpic cells, TNF-α, IL-1, and IL-6 were significantly elevated in the immunostimulated group ($P < 0.05$); these three inflammatory mediators were also significantly higher in CAL-27 cells than in normal cells ($P < 0.05$ for TNF-α and IL-6). Furthermore, TNF-α and IL-6 expression levels in immunostimulated cells were significantly higher than in CAL-27 cells, while the intergroup difference for IL-1 was not statistically significant.

Correlation analysis between gene expression (ODC1, PLAUR, ERRFI1) and inflammatory factors (TNF-α, IL-1, IL-6) in vitro

As shown in the **Figure 8**. For ODC1, there is a strong positive correlation with TNF-α (R =

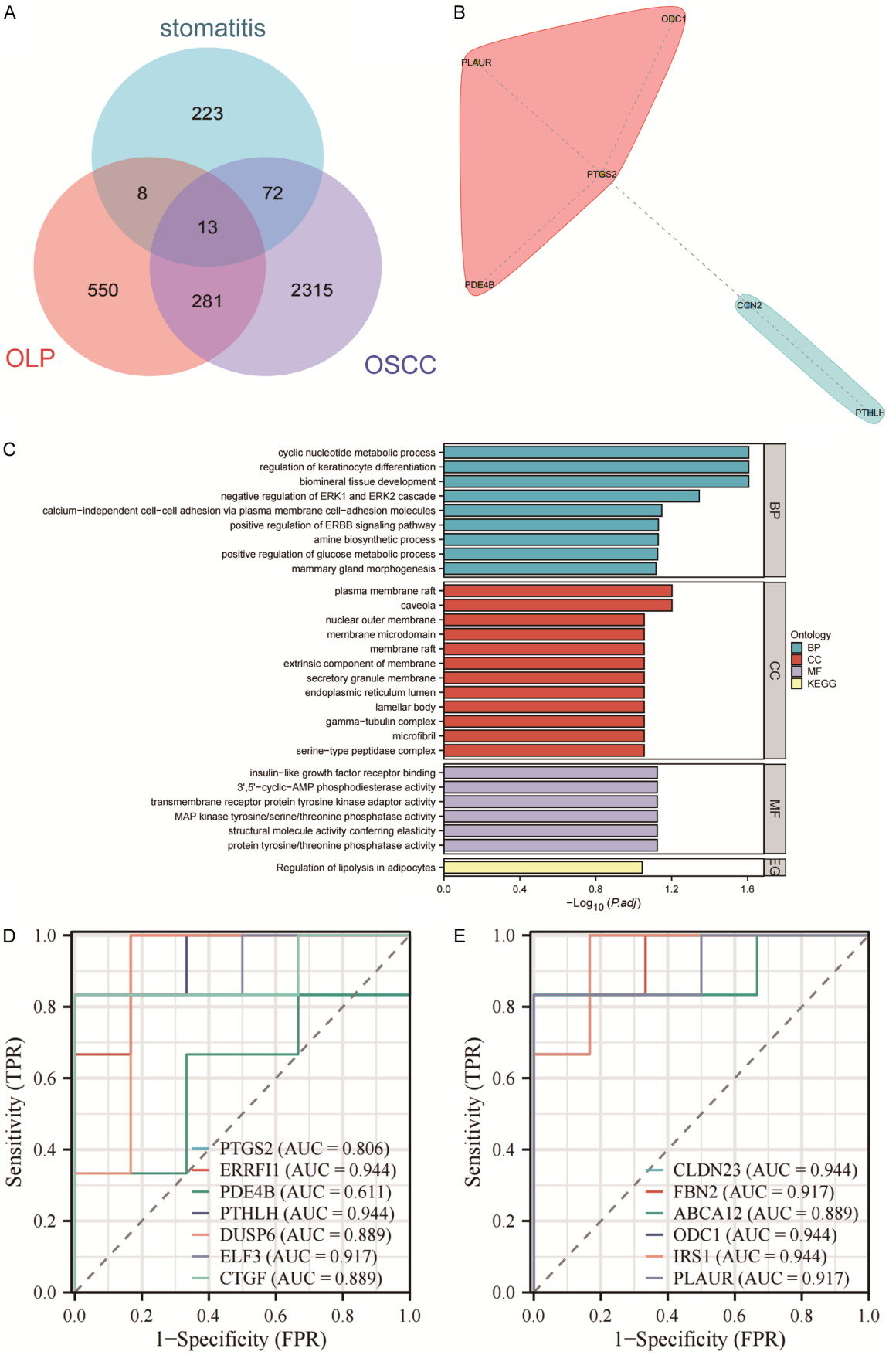
A
stomatitis
223
8
72
13
550
281
2315
OLP
OSCC
B
ODC1
PLAUR
PTGS2
PDE4B
CGN2
PTHLH
C
cyclic nucleotide metabolic process
regulation of keratinocyte differentiation
biomineral tissue development
negative regulation of ERK1 and ERK2 cascade
calcium−independent cell−cell adhesion via plasma membrane cell−adhesion molecules
positive regulation of ERBB signaling pathway
amine biosynthetic process
positive regulation of glucose metabolic process
mammary gland morphogenesis
plasma membrane raft
caveola
nuclear outer membrane
membrane microdomain
membrane raft
extrinsic component of membrane
secretory granule membrane
endoplasmic reticulum lumen
lamellar body
gamma−tubulin complex
microfibril
serine−type peptidase complex
insulin−like growth factor receptor binding
3',5'−cyclic−AMP phosphodiesterase activity
transmembrane receptor protein tyrosine kinase adaptor activity
MAP kinase tyrosine/serine/threonine phosphatase activity
structural molecule activity conferring elasticity
protein tyrosine/threonine phosphatase activity
Regulation of lipolysis in adipocytes
BP
CC
MF
KEGG
Ontology
0.0
0.4
0.8
1.2
1.6
−Log10 (P.adj)
D
Sensitivity (TPR)
1−Specificity (FPR)
PTGS2 (AUC = 0.806)
ERRFI1 (AUC = 0.944)
PDE4B (AUC = 0.611)
PTHLH (AUC = 0.944)
DUSP6 (AUC = 0.889)
ELF3 (AUC = 0.917)
CTGF (AUC = 0.889)
E
Sensitivity (TPR)
1−Specificity (FPR)
CLDN23 (AUC = 0.944)
FBN2 (AUC = 0.917)
ABCA12 (AUC = 0.889)
ODC1 (AUC = 0.944)
IRS1 (AUC = 0.944)
PLAUR (AUC = 0.917)

Figure 4. Identification and characterization of common differentially expressed genes across chronic inflammation, OLP, and OSCC. A. Venn diagram showing overlap of differentially expressed genes among chronic inflammation, OLP, and OSCC, identifying 13 common genes. B. Protein-protein interaction (PPI) network of the 13 intersecting genes constructed using STRING database (confidence score > 0.4) and visualized with Cytoscape, revealing two functional modules centered around PTGS2 and CCN2. C. GO and KEGG functional enrichment analysis of the 13 intersecting genes, showing significantly enriched biological processes, cellular components, molecular functions, and KEGG pathways ($P < 0.05$). D. ROC curves showing diagnostic efficacy of PTGS2, ERRFI1, PDE4B, PTHLH, DUSP6, ELF3, and CTGF, with area under the curve (AUC) values indicated. E. ROC curves showing diagnostic efficacy of CLDN23, FBN2, ABCA12, ODC1, IRS1, and PLAUR, with AUC values indicated.

0.825, $P < 0.001$), IL-1 ($R = 0.692$, $P < 0.001$), and IL-6 ($R = 0.808$, $P < 0.001$). Similarly, PLAUR shows significant positive correlations with TNF-α ($R = 0.775$, $P < 0.001$), IL-1 ($R = 0.810$, $P < 0.001$), and IL-6 ($R = 0.826$, $P < 0.001$). ERRFI1 also exhibits strong positive correlations with TNF-α ($R = 0.677$, $P < 0.001$), IL-1 ($R = 0.566$, $P < 0.001$), and IL-6 ($R = 0.656$, $P < 0.001$).

Discussion

In this study, we systematically investigated the molecular continuum from chronic oral inflammation to OLP and finally to OSCC, identifying 13 genes with persistent dysregulation across all three stages. The progressive expression changes observed - from inflammatory conditions through premalignant lesions to established cancer - support the concept of inflammation-driven carcinogenesis in oral mucosa. PPI network analysis revealed two functionally distinct modules: an "inflammation-proliferation module" centered around PTGS2 (COX-2) including PLAUR and ODC1, and an "ECM-growth factor module" comprising CCN2 and PTHLH. Functional enrichment analysis showed these genes participate in cyclic nucleotide metabolism, keratinocyte differentiation, and ERK1/2 signaling regulation [13]. Using LASSO-logistic regression, we constructed a three-gene (PLAUR, ERRFI1, ODC1) prediction model that demonstrated excellent discriminatory ability (AUC = 0.93) for malignant transformation risk. The progressive upregulation of these genes across the disease continuum - from normal mucosa through OLP to OSCC - was validated in both in vitro inflammatory cell models and independent clinical tissue samples. These findings provide a molecular basis for assessing malignant risk in OLP patients and raise the possibility of targeted intervention.

Mechanistically, the COX-2-centered module plays a pivotal role in inflammation-driven carcinogenesis. PTGS2 (COX-2) is very rarely expressed in normal oral mucosa but significantly overexpressed in more than 92% of OLP lesions [14]. This enzyme promotes angiogenesis, inhibits immune surveillance, and induces epithelial-mesenchymal transition through prostaglandin synthesis, acting as a bridge from chronic inflammation to tumor progression [15, 16]. Our research results reveal the upregulation of PTGS2 in all three conditions, supporting its key role in this transformation process. In addition, the joint upregulation of PDE4B and ODC1 may cooperate to amplify proliferation signals: PDE4B enhances inflammatory pathways by degrading cAMP, thereby modulating PKA signaling and immune responses ; ODC1, as a rate-limiting enzyme for polyamine synthesis, drives rapid cell proliferation and has been targeted by chemopreventive agents such as difluoromethylornithine (DFMO) in cancer prevention trials [17]. The continuous upregulation of PLAUR (encoding uPAR) is associated with tumor invasion phenotype and poor prognosis [18-20], and uPAR inhibition has been shown to significantly reduce the migration and invasion ability of oral cancer cells [21]. The synergistic dysregulation of these genes provides direct molecular evidence for "inflammation-driven carcinogenic effects" and identifies PDE4B, ODC1, and PLAUR as potential therapeutic targets. The clinical relevance of these findings is further supported by the independent clinical cohort, where expression levels of ODC1, PLAUR, and ERRFI1 in normal mucosa, OLP lesions, and OSCC tissues increased in a gradient pattern consistent with disease progression.

The ECM-growth factor module, comprising CCN2 and PTHLH, contributes to tumor progression through microenvironment remodeling. CTGF (CCN2) is frequently overexpressed in chronic inflammation and tumor stroma, promoting ECM deposition, angiogenesis, and lymphangiogenesis [22, 23]. In this study, CTGF

Table 1. Functional annotation of the 13 intersection genes co-expressed in chronic oral inflammation, OLP, and OSCC

No.	Gene	Full name	Function
1	PTGS2	Prostaglandin-endoperoxide Synthase 2 (Cyclooxygenase-2)	Key enzyme in prostaglandin biosynthesis; mediates inflammation and promotes tumorigenic microenvironment
2	ERRFI1	ERBB Receptor Feedback Inhibitor 1	Cytoplasmic adapter that attenuates EGFR/ERBB signaling; functions as a negative feedback regulator of proliferation
3	PDE4B	Phosphodiesterase 4B, cAMP-Specific	Hydrolyzes cAMP, modulating PKA signaling and immune/inflammatory responses; implicated in cancer progression
4	PTHLH	Parathyroid Hormone-Like Hormone	Secreted peptide involved in cell proliferation, bone and cartilage development, and tumor-bone interaction
5	DUSP6	Dual Specificity Phosphatase 6	MAPK phosphatase that inactivates ERK1/2; part of negative feedback loop controlling cell growth and differentiation
6	ELF3	E74 Like ETS Transcription Factor 3	Epithelium-specific transcription factor governing differentiation and cytokine responses; overexpressed in epithelial tumors
7	CTGF	Connective Tissue Growth Factor	Matricellular protein stimulating ECM production, fibrosis, angiogenesis and cancer cell migration
8	CLDN23	Claudin 23	Tight-junction component contributing to epithelial barrier integrity; dysregulation linked to tumor invasion
9	FBN2	Fibrillin 2	Extracellular matrix glycoprotein essential for microfibril assembly and tissue elasticity; participates in EMT
10	ABCA12	ATP-Binding Cassette Subfamily A Member 12	Lipid transporter required for epidermal lipid barrier formation; aberrant expression associated with carcinogenesis
11	ODC1	Ornithine Decarboxylase 1	Rate-limiting enzyme in polyamine biosynthesis, supporting rapid cell proliferation and oncogenic transformation
12	IRS1	Insulin Receptor Substrate 1	Central adaptor of insulin/IGF signaling pathways, regulating metabolism, growth and survival; oncogenic when hyper-activated
13	PLAUR	Plasminogen Activator, Urokinase Receptor	Cell-surface receptor (uPAR) that binds uPA to promote pericellular proteolysis, invasion, and metastasis

Note: Genes were identified from the intersection of differentially expressed genes across three datasets (GSE28035, GSE52130, GSE74530) as shown in **Figure 4A**. Functional annotations were derived from NCBI Gene database and published literature. These 13 genes represent persistently dysregulated transcripts across the inflammation-OLP-OSCC continuum.

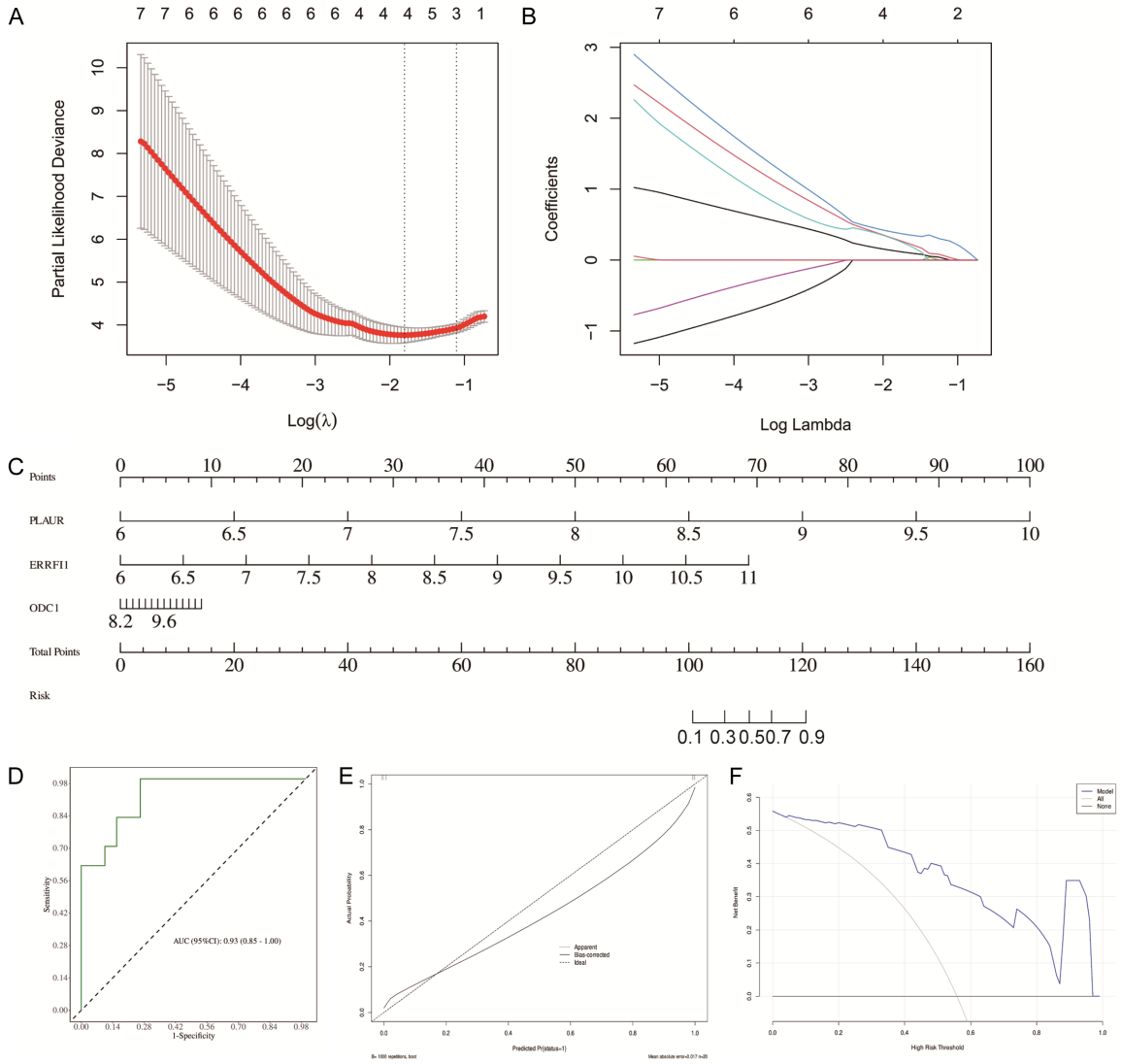

Figure 5. Construction and validation of a three-gene malignant transformation prediction model using LASSO-logistic regression. A. Cross-validation curve of LASSO regression showing the relationship between log(λ) and partial likelihood deviance; the optimal λ value (log[λ] ≈ -2.1) minimizing cross-validation error was selected. B. LASSO coefficient trajectory plot showing coefficient profiles of candidate genes as λ varies; three genes (PLAUR, ERRFI1, ODC1) retained non-zero coefficients at the optimal λ. C. Scatter plot of risk scores calculated from the logistic regression model based on PLAUR, ERRFI1, and ODC1 expression (n = 12). D. Receiver operating characteristic (ROC) curve of the prediction model, showing area under the curve (AUC) = 0.93 (95% confidence interval: 0.85-1.00). E. Calibration curve comparing model-predicted probabilities with observed outcomes; the diagonal line represents perfect prediction, with a mean absolute error of approximately 0.07. F. Decision curve analysis showing the net benefit of the prediction model across threshold probability ranges (0.05-0.75), demonstrating superior clinical utility compared to "treat all" or "treat none" strategies.

was significantly enriched in OSCC tissue, consistent with previous reports demonstrating its role in promoting tongue cancer progression. Notably, DUSP6, which is negatively regulated by the ERK pathway, was identified as a co-expressing gene, and its upregulation may constitute feedback inhibition of excessive CTGF signaling [24, 25]. This balance mechanism could potentially delay malignant transformation during the OLP stage, whereas in OSCC, feedback failure may lead to uncontrolled signal amplification [26]. PTHLH is a key factor in promoting bone invasion and is typically overexpressed in OSCC cases involving the mandibular bone [25]. The simultaneous upregulation of CTGF and PTHLH demonstrates that chronic

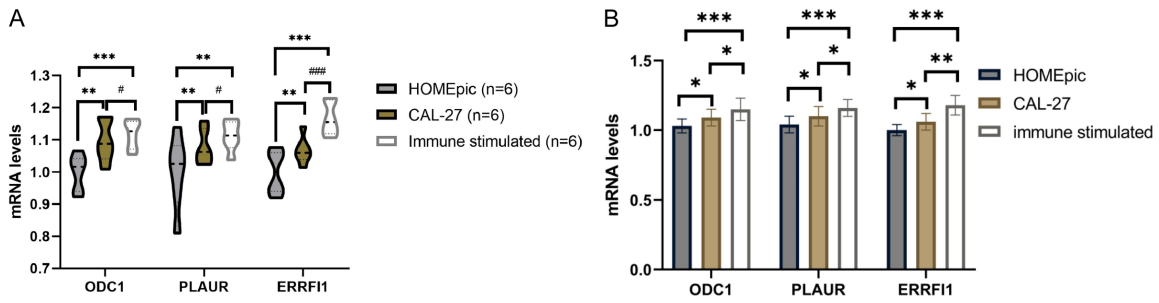

Figure 6. Experimental validation of ODC1, PLAUR, and ERRFI1 expression in cell models and clinical samples. A. Relative mRNA expression levels in normal oral epithelial cells (HOMEpic), immune-stimulated HOMEpic cells, and CAL-27 OSCC cells measured by qRT-PCR. Data are presented as mean ± SD (n = 6 per group). Statistical analysis was performed using one-way ANOVA with Tukey's post-hoc test. *P < 0.05, **P < 0.01, ***P < 0.001 compared to normal HOMEpic; #P < 0.05, ###P < 0.001 comparing immune-stimulated group to CAL-27 group. B. Relative mRNA expression levels in clinical tissue samples: normal oral mucosa (NOM, n = 6), OLP lesions (n = 6), and OSCC tissues (n = 6). *P < 0.05, **P < 0.01, ***P < 0.001 as indicated by brackets, showing a gradient increase across the disease continuum.

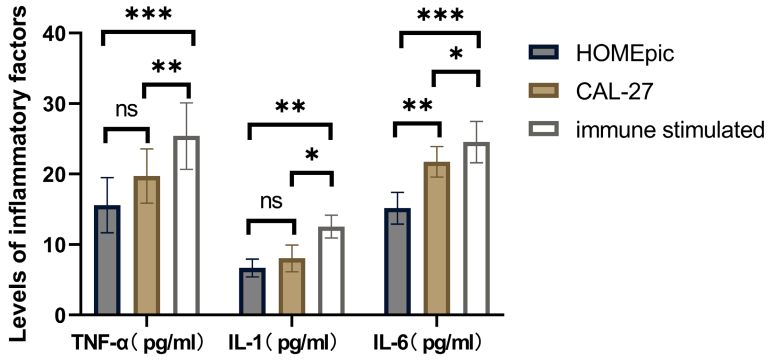

Figure 7. The levels of inflammatory factors TNF-α IL-1, and IL-6 were measured in normal oral epithelial cells (HOMEpic), oral squamous carcinoma cells (CAL-27), and immune-stimulated oral epithelial cells using [Specific Assay Method, e.g., ELISA]. Each group consisted of six biological replicates (n = 6). Statistical significance between groups is denoted as follows: "" indicates significant differences between groups ("*" for P < 0.05, "**" for P < 0.01, "***" for P < 0.001); "ns" indicates no significant difference.

inflammation not only directly affects epithelial cells but also indirectly promotes malignant transformation by remodeling the matrix microenvironment. Furthermore, our data suggest a bidirectional relationship between inflammation and gene dysregulation: inflammatory cytokines (TNF-α, IL-1, IL-6) induce expression of PLAUR, ODC1, and ERRFI1, while their strong positive correlations (R > 0.6, P < 0.001) indicate these genes may amplify inflammatory signaling, creating a positive feedback loop that drives malignant progression. The upregulation of ERRFI1, a negative feedback regulator of EGFR signaling, may appear counterintuitive in carcinogenesis. However, its elevation likely represents a compensatory feedback response to chronic inflammation-induced EGFR pathway activation [27], similar to the "tumor suppressor paradox" observed in early stages of other cancers where negative regulators are transiently upregulated before being silenced during full malignant transformation.

Compared with previously reported OLP malignant transformation biomarkerssuch as CD146 and FAM3B [28], our three-gene model offers several distinct advantages: (1) It captures multiple biological processes simultaneously - proteolysis via PLAUR, proliferation via ODC1, and growth factor signaling via ERRFI1; (2) It was identified through systematic integration of three disease states (inflammation, OLP, OSCC) rather than single pairwise comparisons, ensuring relevance across the entire continuum; (3) It was validated in both in vitro inflammatory models and independent clinical samples, demonstrating robustness; and (4) The three genes have well-established roles in inflammation and cancer, providing mechanistic plausibility. For clinical translation, detection of these biomarkers in tissue biopsies could guide risk stratification and surveillance intensity for OLP patients. Importantly, given that PLAUR encodes a soluble receptor (suPAR) detectable in blood and saliva [29],

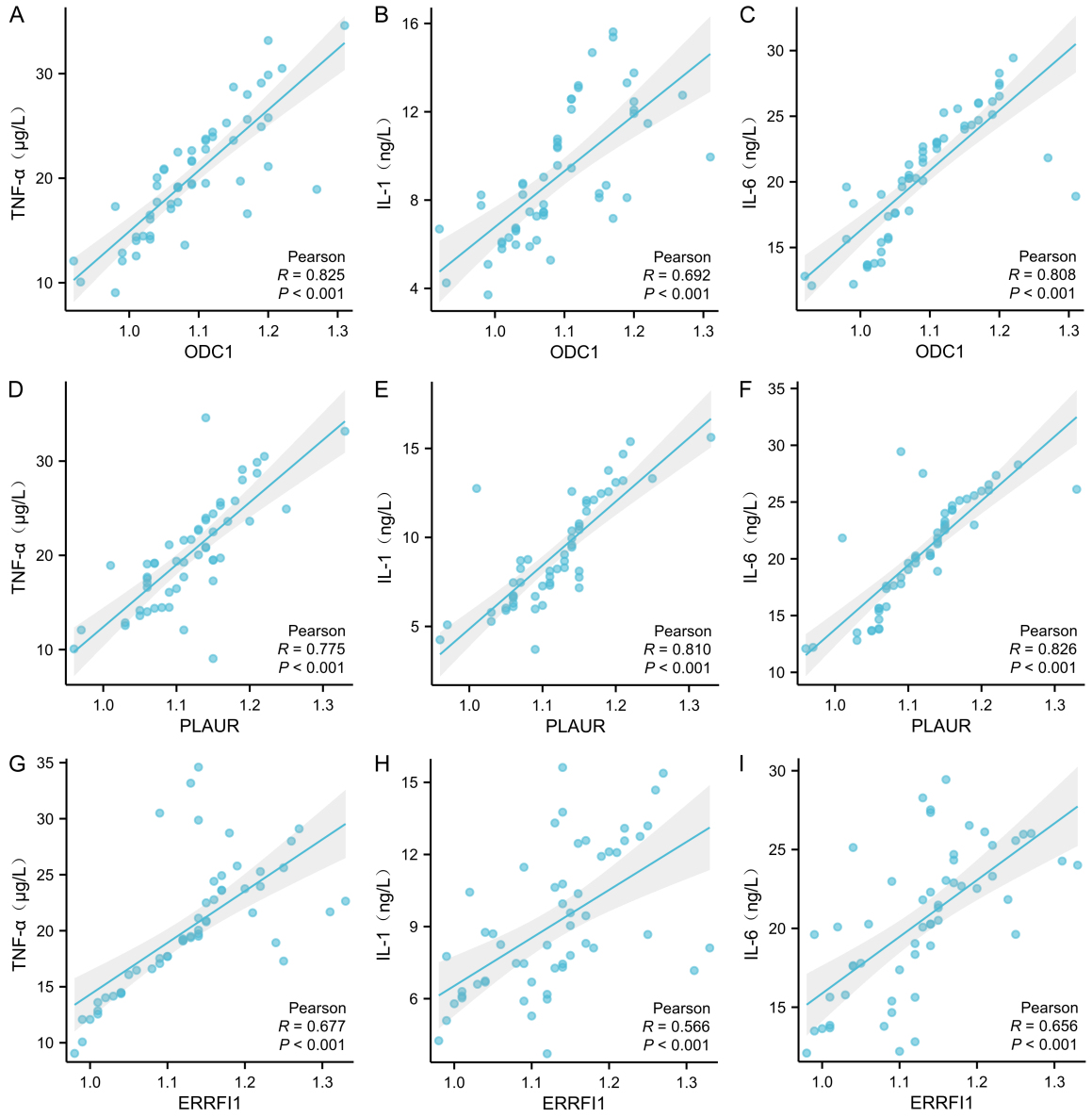

Figure 8. Correlation analysis between mRNA expression levels of ODC1, PLAUR, and ERRFI1 and inflammatory factors TNF-α, IL-1, and IL-6. The mRNA expression levels of ODC1, PLAUR, and ERRFI1 were quantified by qRT-PCR, and the levels of inflammatory factors TNF-α, IL-1, and IL-6 were measured using in relevant cell types. Pearson correlation analysis was performed to assess the relationships. The Pearson correlation coefficient (R) and *P*-values are indicated within each plot. A significant positive correlation is observed between the expression levels of these genes and the inflammatory factors, with R values ranging from moderate to strong and all P < 0.001, suggesting a potential association between gene expression and inflammatory responses.

and polyamines (ODC1 enzymatic products) are measurable in oral fluids, our findings raise the possibility of developing non-invasive saliva-based tests for monitoring malignant transformation risk. Such tests would greatly enhance clinical utility and patient compliance, enabling regular monitoring without the need for repeated biopsies [30, 31]. Future prospective studies should evaluate the predictive performance of this three-gene signature in larger cohorts and explore its utility in guiding clinical decision-making for OLP patients at risk of malignant transformation.

However, there are certain limitations in this study: first, the analysis depends on public transcriptome data, and the sample size and batch variation may affect the detection of low-

abundance genes [32]. Secondly, the screening criteria for co-expressed genes are relatively strict, and genes that only work at a specific stage may be ignored. Additionally, the LASSO-logistic regression model was constructed using a relatively small discovery cohort (n = 12), which increases the risk of overfitting. Although repeated 10-fold cross-validation yielded a mean AUC of 0.89 (SD = 0.06) suggesting reasonable stability, the high AUC value of 0.93 in the training set requires validation in a large, independent external cohort. Therefore, we have softened our conclusions throughout the manuscript, describing the model as showing "promising predictive capability" rather than "effective prediction", and emphasize that these findings should be considered preliminary until validated in larger, multicenter prospective studies. Finally, although the correlation between inflammatory factors and key genes has been observed, their causal regulatory relationship has not been confirmed by functional experiments. Future work should not only verify the predictive efficacy of the biomarker panel in prospective clinical cohorts but also establish the optimal probability threshold for clinical decision-making through multicenter collaborations, and assess its performance across different clinical scenarios. In addition, in vitro and in vivo models are needed to further clarify the specific mechanisms by which PLAUR, ODC1, and ERRFI1 drive the progression from inflammation to cancer.

Conclusion

This study reveals the key molecular link between chronic oral inflammation, OLP and OSCC. Thirteen key genes have been identified, especially PTGS2, PLAUR, ERRFI1 and ODC1, which have been revealed to be potential drivers of inflammatory-induced malignant transformation. Prediction models based on PLAUR, ERRFI1 and ODC1 showed good diagnostic accuracy in internal validation (AUC = 0.93) and were verified by qRT-PCR experiments. These findings provide promising biomarkers and therapeutic targets for assessing and managing the risk of malignant transformation in OLP patients, which are worthy of further prospective and mechanistic research.

Disclosure of conflict of interest

None.

Address correspondence to: Bingjie Wang, Department of Stomatology, The Affiliated People's Hospital of Ningbo University, No. 251, Baizhang East Road, Yinzhou District, Ningbo 315000, Zhejiang, China. E-mail: rmwangbingjie@nbu.edu.cn

References

[1] de Lanna CA, da Silva BNM, de Melo AC, Bonamino MH, Alves LDB, Pinto LFR, Cardoso AS, Antunes HS, Boroni M and Cohen Goldemberg D. Oral lichen planus and oral squamous cell carcinoma share key oncogenic signatures. Sci Rep 2022; 12: 20645.

[2] Warnakulasuriya S, Kujan O, Aguirre-Urizar JM, Bagan JV, González-Moles M, Kerr AR, Lodi G, Mello FW, Monteiro L, Ogden GR, Sloan P and Johnson NW. Oral potentially malignant disorders: a consensus report from an international seminar on nomenclature and classification, convened by the WHO Collaborating Centre for Oral Cancer. Oral Dis 2021; 27: 1862-1880.

[3] Sung H, Ferlay J, Siegel RL, Laversanne M, Soerjomataram I, Jemal A and Bray F. Global cancer statistics 2020: GLOBOCAN estimates of incidence and mortality worldwide for 36 cancers in 185 countries. CA Cancer J Clin 2021; 71: 209-249.

[4] Sasahira T and Kirita T. Hallmarks of cancer-related newly prognostic factors of oral squamous cell carcinoma. Int J Mol Sci 2018; 19: 2413.

[5] Chen SH, Hsiao SY, Chang KY and Chang JY. New insights into oral squamous cell carcinoma: from clinical aspects to molecular tumorigenesis. Int J Mol Sci 2021; 22: 2252.

[6] González-Moles MÁ and Ramos-García P. An evidence-based update on the potential for malignancy of oral lichen planus and related conditions: a systematic review and meta-analysis. Cancers (Basel) 2024; 16: 608.

[7] Mehdipour M, Shahidi M, Anbari F, Mirzaei H, Jafari S, Kholghi A, Lotfi E, Manifar S and Mashhadiabbas F. Salivary level of microRNA-146a and microRNA-155 biomarkers in patients with oral lichen planus versus oral squamous cell carcinoma. BMC Oral Health 2023; 23: 433.

[8] Xie F, Gleue CA, Deschaine M, Dasari S, Sartori-Valinotti JC, Charlesworth MC, Meves A and Lehman JS. Differential proteomic expression in indolent versus transforming oral lichen planus. Exp Dermatol 2023; 32: 502-510.

[9] Pariyawathee S, Phattarataratip E and Thongprasom K. CD146 expression in oral lichen planus and oral cancer. Clin Oral Investig 2020; 24: 325-332.

[10] Wang W, Wang M, Ahmed MMS, Zhao Y, Wu H, Musa M and Chen X. FAM3B serves as a bio-

marker for the development and malignancy of oral lichen planus. Int J Gen Med 2022; 15: 763-776.
[11] Keim-Del Pino C, Ramos-García P and González-Moles MÁ. A molecular hypothesis on malignant transformation of oral lichen planus: a systematic review and meta-analysis of cancer hallmarks expression in this oral potentially malignant disorder. Cancers (Basel) 2024; 16: 2614.
[12] Rabiu L, Chinn M, Chen F, Yerkinkazhina Y, Tian Y and Zhu WG. Targeting inflammation and immune regulation in chronic inflammation associated cancers. Cancer Sci 2026; [Epub ahead of print]
[13] Alrashdan MS, Cirillo N and McCullough M. Oral lichen planus: a literature review and update. Arch Dermatol Res 2016; 308: 539-551.
[14] Ladjevac N, Milovanovic M, Jevtovic A, Arsenijevic D, Stojanovic B, Dimitrijevic Stojanovic M, Stojanovic B, Arsenijevic N, Arsenijevic A and Milovanovic J. The role of IL-17 in the pathogenesis of oral squamous cell carcinoma. Int J Mol Sci 2023; 24: 9874.
[15] Niklander SE. Inflammatory mediators in oral cancer: pathogenic mechanisms and diagnostic potential. Front Oral Health 2021; 2: 642238.
[16] Bruno A, Tacconelli S, Contursi A, Ballerini P and Patrignani P. Cyclooxygenases and platelet functions. Adv Pharmacol 2023; 97: 133-165.
[17] Baby TK, Bindhu PR, Pillai RK and Jayanthi P. Immunohistochemical expression of cyclooxygenase-2 in oral lichen planus and normal oral mucosa. Indian J Pathol Microbiol 2022; 65: 8-12.
[18] Finetti F, Travelli C, Ercoli J, Colombo G, Buoso E and Trabalzini L. Prostaglandin E2 and cancer: insight into tumor progression and immunity. Biology (Basel) 2020; 9: 434.
[19] Finetti F, Paradisi L, Bernardi C, Pannini M and Trabalzini L. Cooperation between prostaglandin E2 and epidermal growth factor receptor in cancer progression: a dual target for cancer therapy. Cancers (Basel) 2023; 15: 2374.
[20] Agraval H, Sharma JR, Prakash N and Yadav UCS. Fisetin suppresses cigarette smoke extract-induced epithelial to mesenchymal transition of airway epithelial cells through regulating COX-2/MMPs/β-catenin pathway. Chem Biol Interact 2022; 351: 109771.
[21] Bevanda M, Kelam N, Racetin A, Filipović N, Bevanda Glibo D, Bevanda I and Vukojević K. Expression pattern of PDE4B, PDE4D, and SFRP5 markers in colorectal cancer. Medicina (Kaunas) 2024; 60: 1202.
[22] Tang J, Wu X, Cheng B and Lu Y. Identification of a polyamine-related signature and six novel prognostic biomarkers in oral squamous cell carcinoma. Front Mol Biosci 2023; 10: 1073770.
[23] Ghosh P, Dey A, Nandi S, Majumder R, Das S and Mandal M. CTGF (CCN2): a multifaceted mediator in breast cancer progression and therapeutic targeting. Cancer Metastasis Rev 2025; 44: 32.
[24] Mahmood N, Mihalcioiu C and Rabbani SA. Multifaceted role of the urokinase-type plasminogen activator (uPA) and its receptor (uPAR): diagnostic, prognostic, and therapeutic applications. Front Oncol 2018; 8: 24.
[25] Hashiguchi S, Tanaka T, Mano R, Kondo S and Kodama S. CCN2-induced lymphangiogenesis is mediated by the integrin αvβ5-ERK pathway and regulated by DUSP6. Sci Rep 2022; 12: 926.
[26] Okusha Y, Eguchi T, Tran MT, Sogawa C, Yoshida K, Itagaki M, Taha EA, Ono K, Aoyama E, Okamura H, Kozaki KI, Calderwood SK, Takigawa M and Okamoto K. Extracellular vesicles enriched with moonlighting metalloproteinase are highly transmissive, pro-tumorigenic, and trans-activates cellular communication network factor (CCN2/CTGF): CRISPR against cancer. Cancers (Basel) 2020; 12: 881.
[27] Shah AM, Jain K, Desai RS, Bansal S, Shirsat P, Prasad P and Bodhankar K. The role of increased connective tissue growth factor in the pathogenesis of oral submucous fibrosis and its malignant transformation-an immunohistochemical study. Head Neck Pathol 2021; 15: 817-830.
[28] Shen YW, Zhou YD, Chen HZ, Luan X and Zhang WD. Targeting CTGF in cancer: an emerging therapeutic opportunity. Trends Cancer 2021; 7: 511-524.
[29] Minaei E, Mueller SA, Ashford B, Thind AS, Mitchell J, Perry JR, Genenger B, Clark JR, Gupta R and Ranson M. Cancer progression gene expression profiling identifies the urokinase plasminogen activator receptor as a biomarker of metastasis in cutaneous squamous cell carcinoma. Front Oncol 2022; 12: 835929.
[30] Yi SA, Cho D, Kim S, Kim H, Choi MK, Choi HS, Shin S, Yun S, Lim A, Jeong JK, Yoon DE, Cha HJ, Kim K, Han JW, Cho HS and Cho J. Functional loss of ERBB receptor feedback inhibitor 1 (MIG6) promotes glioblastoma tumorigenesis by aberrant activation of epidermal growth factor receptor (EGFR). Mol Oncol 2025; 19: 937-953.
[31] Jin R, Li H, Nan S and Wang H. FOXA1 co-activates circODC1 and ODC1 in HPV-positive cervical cancer cell growth. Syst Biol Reprod Med 2024; 70: 113-123.
[32] Zhang Y, Qu W, Yan R, Liu H, Zhang C, Li Z and Dong G. A reliable and quick method for screening alternative splicing variants for low-abundance genes. PLoS One 2024; 19: e0305201.